A Renormalisation Approach to Reaction-Diffusion Processes on Fractals

Janan Abdulbake[†], Anthony J. Mulholland[‡] and Jagannathan Gomatam [†]

†Department of Mathematics, Glasgow Caledonian University, Glasgow, U.K.
‡ Department of Mathematics, University of Strathclyde, Glasgow, U.K.

Abstract

Of fundamental importance to wave propagation in a wide range of physical phenomena is the structural geometry of the supporting medium. Recently there have been several investigations on wave propagation in fractal media. We present here a renormalisation approach to the study of reaction-diffusion wave propagation on finitely ramified fractal structures. In particular we will study a Rinzel-Keller type model, supporting travelling waves on a Sierpinski gasket lattice.

1. Introduction

The role that fractal structures play on the dynamics of wave propagation is investigated in this paper. A recent and very powerful advance in the understanding of wave propagation in complex structures is due to the realisation that, in certain circumstances, these structures are self-similar [1]. There is a very wide and diverse literature on the propagation of waves in various Euclidean media and therefore there is motivation to investigate the effect that fractal geometry will have on the nature of these waveforms. It has been well recognised, that the geometrical properties of the medium has a marked effect upon the wave propagating in it [2, 3]. The geometries can be classified as one of two types. The first is where there exists a fractal interface, which can act as an impenetrable boundary to some homogeneous transporting medium or as the interface between two different homogeneous phases. The second is where the transporting medium itself is fractal, for instance, a mass fractal or a fractal lattice, the latter case being of central importance in this paper.

There have been several investigations on the effect that a fractal medium has on the process of diffusion, so called anomalous diffusion [4], and a number of studies of coupled Reaction-Diffusion equations on fractal supports with diffusion limited annihilation type kinetics [5, 6]. The gaps which evolve between domains of segregated particles, the so called interparticle distribution function, is described in terms of scaling laws related to the fractal dimension of the support. Global information is also obtained, such as particle densities over time. Scalar Reaction-Diffusion models involving coagulation and annihilation dynamics can be tractable and afford an accurate description of "anomalous diffusion" on fractals and the evolution of the interparticle distribution function [7]. By examining the asymptotic behaviour of these systems a generalised scaling law can be derived for the mean square displacement [8]. In this paper however we are interested in models with

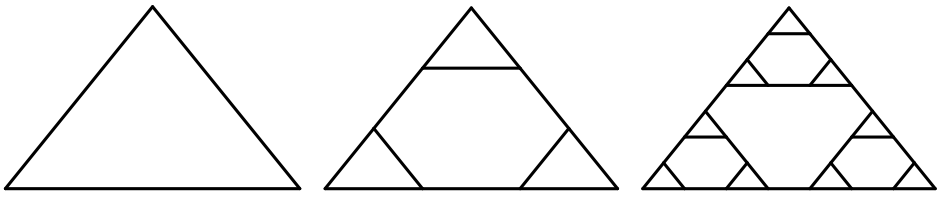

Figure 1: The pre-fractals E_0, E_1 and E_2 for the $SG(3)$ lattice.

excitable kinetics and address the question of the existence of travelling waves. Using probability theory and renormalisation methods it is possible to derive analytic solutions in terms of recursion relationships for the diffusion process on the Sierpinski Gasket [9]. Recently there have been more general investigations on wave propagation in fractal media [10]-[17]. These highly heterogeneous but yet deterministic fractal structures provide a framework for the study of the geometric phase transitions found in percolation theory [18] or in the investigation of reacting and diffusing chemical species in a solid catalyst [19]. In particular, there have been a series of papers devoted to transport equations with first order reaction schemes in a class of deterministic fractal media [20]-[30]. This approach is particularly exciting and provides one of the few analytical descriptions of the dynamics of wave propagation in fractal lattices. In this paper we will extend this method to examine the effect of fractal geometry on the propagation of excitable reaction-diffusion waves. In Section 2 we show that the Sierpinski Gasket lattice ($SG(3)$) (see Figure 1) can support reaction-diffusion waves. These waves are then described in Section 3 by means of a renormalisation framework. In Section 4 the renormalisation methodology is used to analyse travelling waves on finite generation level lattices.

2. Reaction-Diffusion Systems in Excitable Media.

In this section we will discuss excitable reaction-diffusion (RD) systems and in particular the Rinzel-Keller model (RK) [31] which provides analytical expressions for travelling pulses and periodic wavetrains in Euclidean media. The fundamental assumption in the Rinzel-Keller model is that the nonlinear kinetics can be approximated by a piecewise linear function. The piecewise linear caricature of the cubic kinetics results in a Reaction-Diffusion system which is qualitatively the same. One subtle difference arises when we examine the dependency of the wave speed c on the kinetic parameter a. As $a \to 0^+$ the wave speed is finite for cubic kinetics but becomes unbounded in the piecewise linear case [32]. As a guide to the possible wave forms which the $SG(3)$ can support we have numerically solved the Rinzel-Keller model, using finite differences, at a low generation level. In the next section, we will detail the fundamental equations which will provide the basis of the renormalisation process we have developed to analyse a travelling wave solution to the RK model in the $SG(3)$.

The general form of a reaction-diffusion system in isotropic media is [33],

$$\frac{\partial \underline{v}}{\partial t} = D\nabla^2 \underline{v} + \underline{f}(\underline{v}) \tag{1}$$

where $\underline{v} = \underline{v}(\underline{x}, t) \in \mathbb{R}^m$, is the vector of reactants, $\underline{f} : \mathbb{R}^m \to \mathbb{R}^m$ are the reaction kinetic

terms, D is the diffusion coefficient, and $(\underline{x}, t) \in (\mathbb{R}^m, \mathbb{R}^+)$. The vector $\underline{v}$ can represent, for example, the concentrations of m chemical species. Of particular relevance to this report is the RK model which is used in the study of nerve conduction [31],

$$\begin{aligned} \frac{\partial v}{\partial t} &= D\frac{\partial^2 v}{\partial x^2} - g(f(v) + w) \\ \frac{\partial w}{\partial t} &= bv \end{aligned} \tag{2}$$

where the reaction term $f(v)$ is usually of the form $v(a-v)(1-v)$; g and b are the reaction coefficients. The RK model employs the piecewise linear approximation to the reaction term, $f(v) = v - H(v-a)$, $0 \leq a \leq 0.5$, where H denotes the Heaviside step function. The importance of this model is that, due to the piecewise linear approximation of the nonlinearities in the kinetics, it will yield to the renormalisation theory.

2.1 Numerical Solution of a Reaction-Diffusion System in the Sierpinski Gasket lattice SG(3)

In this section we develop a discretisation scheme for the RK model on the $SG(3)$. We demonstrate that it is possible, for low generation levels of the $SG(3)$, to numerically solve the field equations using finite differences. This acts both as a check on our analytic solutions and as an aid to our intuitive understanding of the process.

Let $\underline{v}^{(n)} = \{v_i^{(n)} : i = 1, 2, \ldots, N_n\}$ and $\underline{w}^{(n)} = \{w_i^{(n)} : i = 1, 2, \ldots, N_n\}$ be the concentration vectors at each of the lattice sites i at generation level n. The RK model can then be written as,

$$\begin{aligned} \frac{\partial v_i^{(n)}}{\partial t} &= \epsilon D \nabla^2 v_i^{(n)} - \frac{g}{\epsilon}(f(v_i^{(n)}) + w_i^{(n)}) \\ \frac{\partial w_i^{(n)}}{\partial t} &= bv_i^{(n)} \quad \text{b}\geq 0 \end{aligned} \tag{3}$$

where

$$f(v_i^{(n)}) = \begin{cases} v_i^{(n)} & v_i^{(n)} \leq a \\ v_i^{(n)} - 1 & v_i^{(n)} > a \end{cases} ,$$

$(0 \leq a \leq 0.5)$ is the reaction term. We have introduced a small parameter ϵ which is used to balance the levels of reaction and diffusion. It is the fine balance and interplay of these two factors which give rise to travelling waves. The spatially discretised system in (3) can be written as,

$$\begin{aligned} \frac{\partial v_i^{(n)}}{\partial t} &= \frac{\epsilon D}{\triangle x^2} A^{(n)} v_i^{(n)} - \frac{g}{\epsilon}(f(v_i^{(n)}) + w_i^{(n)}) \\ \frac{\partial w_i^{(n)}}{\partial t} &= bv_i^{(n)} \quad \text{b}\geq 0 \end{aligned} \tag{4}$$

where $A^{(n)}/\triangle x^2$ is a matrix equivalent of the Laplacian operator incorporating the boundary conditions [14]. Neumann boundary conditions are applied at the output nodes, that

is $v_i^{'(n)}|_{A,B,C} = 0$ (see Figure 9). To investigate a travelling wave solution to this initial value problem, a small set of nodes are excited by setting their v values equal to 1 initially. The connectivity of the Sierpinski gasket is captured in the recursion relation (8) but we need to automate the generation of $A^{(n)}$ for our numerical algorithm. We discuss below how this is done and also provide the transformation of this nodal description of wave evolution to Cartesian co-ordinates. The initial adjacency matrix is defined by,

$$H_{ij}^{(1)} = \begin{cases} 0 & i = j \\ 1 & i \neq j \end{cases}$$

and for level n,

$$H_{pq}^{(n)} = \begin{cases} 1 & \text{if } H^{(1)}_{(p-1)mod3+1,(q-1)mod3+1} = 1 \text{ and } \lceil p/3 \rceil = \lceil q/3 \rceil \\ 0 & \text{Otherwise} \end{cases} ,$$

where, $p, q \in \{1, 2, \ldots N_n = 3^n\}$ and the symbol $\lceil x \rceil$ denotes the integer part of x, plus 1. Note that the first condition ensures that the $H^{(1)}$ matrix is repeated to generate $H^{(n)}$, whilst the latter condition ensures that $H^{(n)}$ has a tri-diagonal form. The connection matrix is given recursively by,

$$V_{pq}^{(n)} = \begin{cases} 1 & \text{if } \{p, q\} \in L_n \\ 0 & \text{Otherwise} \end{cases} ,$$

where

$$L_n = \bigcup_{i=2}^{n} W^{(i)}, L_{i-1}, L_{i-1} + 3^{i-1}, L_{i-1} + 2 \times 3^{i-1}, \quad L_2 = W^{(2)}$$

and

$$\begin{aligned} W^{(n)} = \; & \{\{(3^{n-1}+1)/2, 1+3^{n-1}\}, \{3^{n-1}, 1+2\times 3^{n-1}\}, \{2\times 3^{n-1}, (5\times 3^{n-1}+1)/2\}, \\ & \{1+3^{n-1}, (3^{n-1}+1)/2\}, \{1+2\times 3^{n-1}, 3^{n-1}\}, \{(5\times 3^{n-1}+1)/2, 2\times 3^{n-1}\}\} \end{aligned} .$$

The matrix B that represents the boundary nodes in the $SG(3)$, is a sparse matrix given by,

$$B_{pq}^{(n)} = \begin{cases} 1 & \text{if } p = q \text{ and } (p = (3^n+1)/2 \text{ or } p = 3^n) \\ 0 & \text{Otherwise} \end{cases} .$$

For the $SG(3)$, the matrix $A^{(n)}$ can now be written as [14, 21],

$$A_{pq}^{(n)} = H_{pq}^{(n)} + V_{pq}^{(n)} + B_{pq}^{(n)} - 3\delta_{pq} , \tag{5}$$

where δ_{pq} is the identity matrix. By applying the finite difference method the system (4) becomes,

$$\begin{aligned} v_i^{(n),m+1} &= v_i^{(n),m} + \frac{\epsilon \triangle t D}{\triangle x^2} \sum_{j=1}^{N_n} A_{ij}^{(n)} v_j^{(n),m} - \frac{g \triangle t}{\epsilon} (f(v_i^{(n),m}) + w_i^{(n),m}) \\ w_i^{(n),m+1} &= w_i^{(n),m} + b \triangle t v_i^{(n),m} \end{aligned} . \tag{6}$$

where $\triangle x = \dfrac{l}{2^n - 1}$, l is the side length of $SG(3)$,

$$\nabla^2 v_i^{(n),m} = \frac{1}{\triangle x^2} \sum_{j=1}^{N_n} A_{ij}^{(n)} v_j^{(n),m},$$

and m denotes the time step. To represent the wave evolution in the Cartesian co-ordinates, each node in the $SG(3)$, can be transformed at each level n by using the formula,

$$SG^{(n)}(3) = \bigcup_{j=2}^{n} \left\{ \begin{array}{c} SG^{(j-1)}, SG^{(j-1)} + \{2^{(j-1)} l/\triangle x(j), 0\}, \\ SG^{(j-1)} + \{2^{(j-2)} l/\triangle x(j), 2^{(j-1)} a/\triangle x(j)\} \end{array} \right\},$$

where $SG^{(1)}(3) = \{\{0,0\},\{l,0\},\{l/2,a\}\}$ is the Cartesian co-ordinates at level 1, the length scale at generation level n is $\triangle x(n) = \dfrac{l}{2^n - 1}$, the diameter of the $SG(3)$ is l and $a = \dfrac{\sqrt{3}}{2} l$.

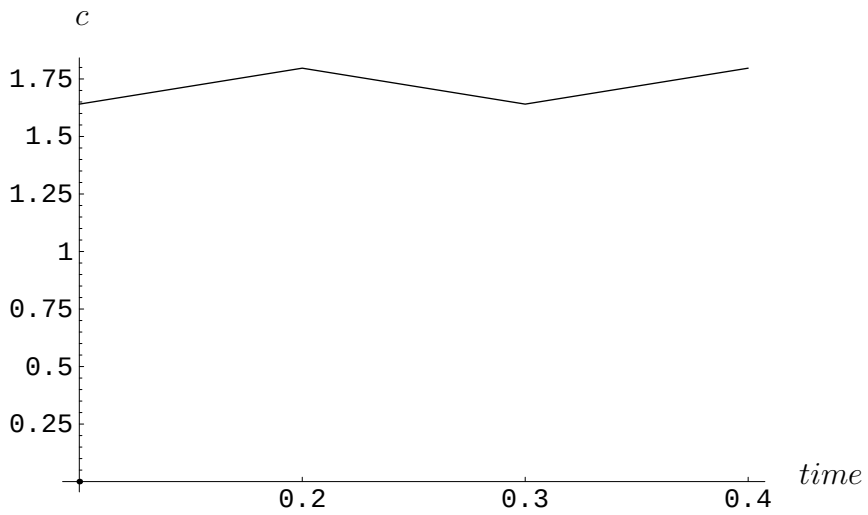

Figure 2: The speed c versus time for a travelling wave on the $SG(3)$ of order $n = 7$, where $\Delta t = 10^{-5}$, $D = 1$, $g = 1$, $a = 0.1$, $\varepsilon = 0.01$, total number of time steps$= 10^4$, $v_1^{(7)} = 1$, $b = 1$.

We have solved (6) numerically and instigated a travelling wave by exciting a number E of the $SG(3)$ nodes. For instance, the initial condition $v_1^{(7)} = 1$ gives rise to the wave profiles shown in Figure 5, which demonstrates that even this most minimal of excitation exceeds the threshold required for wave propagation. We then calculate the wave speed as a function of time. This calculation is performed by identifying the v values along one side of the $SG(3)$. We produced six sets of these values at different instances of time as the wave proceeds. We calculate the gradient of each set by taking the difference between each successive set of values and then identify the position of the maximum gradient. The velocity is calculated by taking the difference between these positions, suitably normalised by dividing by the number of nodes along the edge, over the time taken. We can plot the wave speed versus time and obtain an approximate horizontal line which indicates that this wave is travelling with constant velocity (see Figure 2). The fluctuations are attributable mainly to the coarseness of the time sampling of the wave profile.

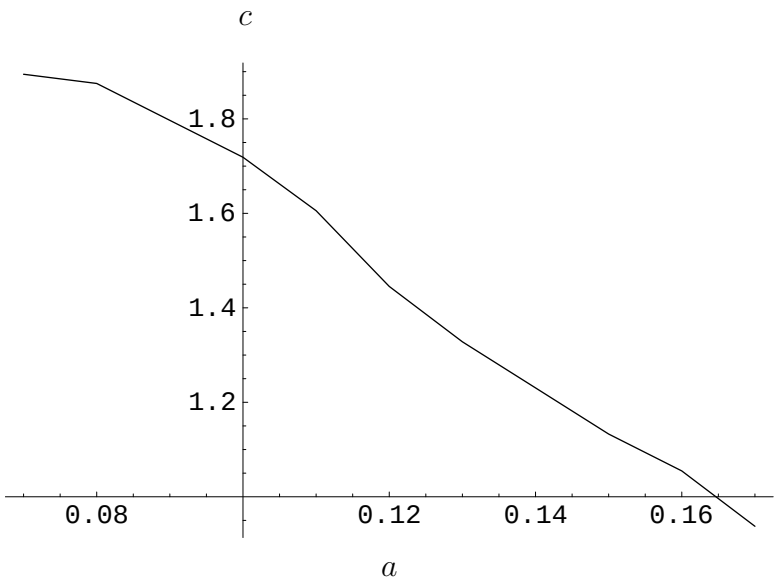

Figure 3: The speed c versus a for a travelling wave along the $SG(3)$ of order $n = 7$, where $\Delta t = 10^{-5}$, $D = 1$, $g = 1$, $b = 1$, $a = 0.1$, $\varepsilon = 0.01$, total number of time steps$= 10^4$ and $v_1^{(7)} = 1$.

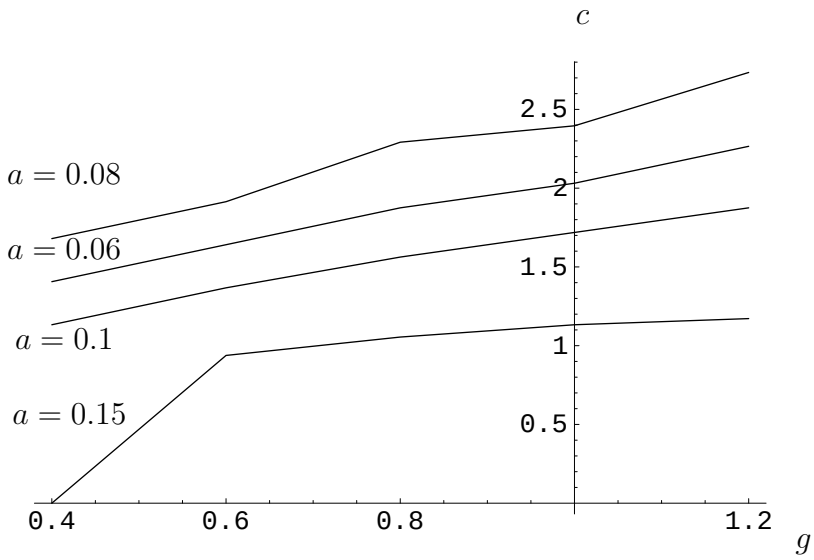

Figure 4: Speed of propagation c of the wave impulse versus g for various values of a where $n = 7$, $\Delta t = 10^{-5}$, $D = 1$, $\varepsilon = 0.01$, total number of time steps$= 10^4$, $v_1^{(7)} = 1$ and $b = 1$.

We have performed a number of such numerical experiments with a variety of initial conditions in order to elucidate the range of waves supported by the structure. We have tried exciting single nodes in the centre of the $SG(3)$ to examine the possibility of expanding target patterns and we have excited single lines of nodes to try and produce spiral patterns. In both cases due to the topology of the structure, the emerging wave quickly assumes the profile of one or several travelling planar waves. Importantly, we have demonstrated that such structures can support travelling reaction-diffusion waves, but due to the topology of the lattice the predominant pattern is a planar wave. It should

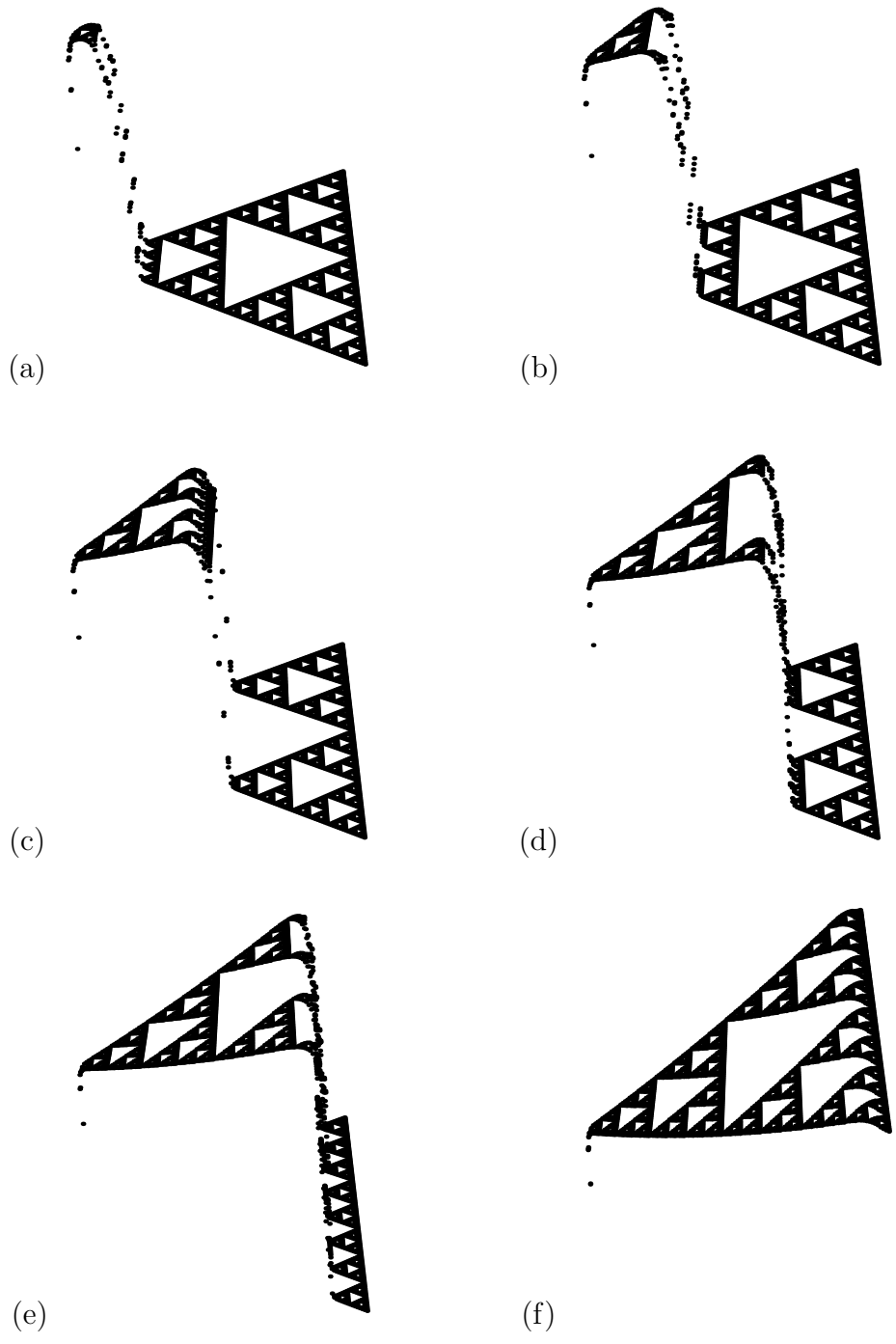

Figure 5: Wave impulse profiles in the Sierpinski Gasket ($n = 7$, $\Delta t = 10^{-5}$, $D = 1$, $g = 1$, $a = 0.1$, $\varepsilon = 0.01$, total number of time steps$= 10^4$, $v_1^{(7)} = 1$, $b = 1$, (a) $t = 0.1s$, (b) $t = 0.2s$, (c) $t = 0.3s$, (d) $t = 0.4s$, (e) $t = 0.5s$ and (f) $t = 0.6s$)

therefore be possible to use a renormalisation methodology to obtain an analytical hold on the interplay between the model parameters and the wave speed. In this way we will be able to investigate the dispersive properties of the $SG(3)$. For low generation levels of the $SG(3)$ we can use the approach in this section to examine the dependency of the wave speed c on some of the parameters in system (6). For example, for $0 < a < 0.18$ a travelling wave exists and its velocity is monotonically decreasing as the value of a is increased (see Figure 3), and for fixed values of a we have produced various curves of c versus g (see Figure 4).

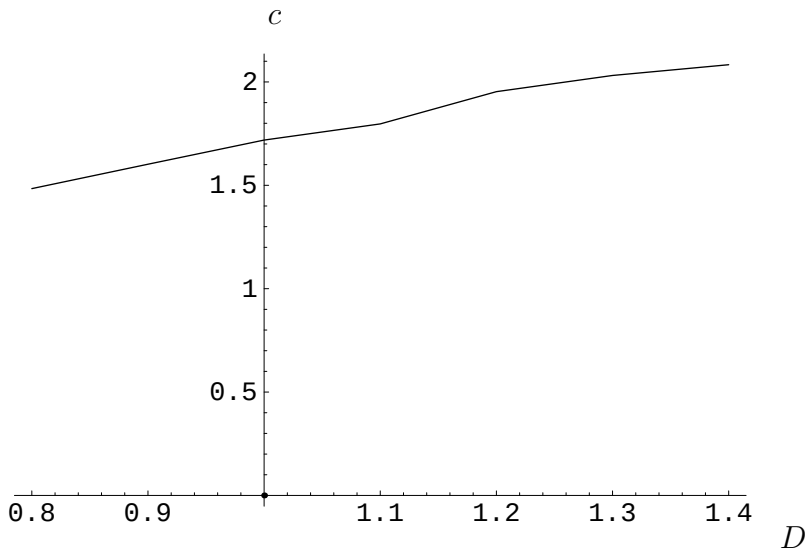

Figure 6: The speed c versus D for a travelling wave on the $SG(3)$ of order $n = 7$, where $\Delta t = 10^{-5}$, $g = 1$, $b = 1$, $a = 0.1$, $\varepsilon = 0.01$, total number of time steps$= 10^4$ and $v_1^{(7)} = 1$.

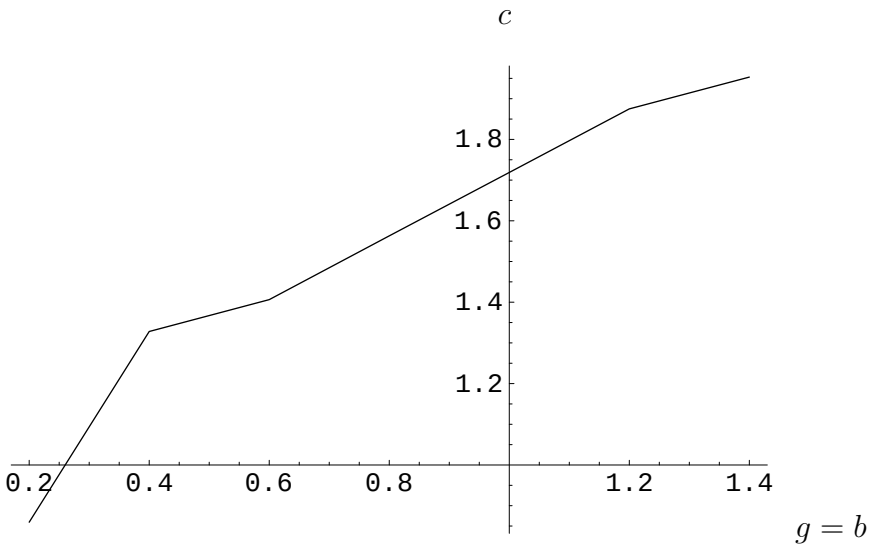

Figure 7: The speed c versus $g = b$ for a travelling wave on the $SG(3)$ of order $n = 7$, where $\Delta t = 10^{-5}$, $D = 1$, $a = 0.1$, $\varepsilon = 0.01$, total number of time steps$= 10^4$ and $v_1^{(7)} = 1$.

It follows that there are bounds on the parameters a, b and g in order for such travelling wave to exist. In fact we were unable to realise a travelling wave on the $SG(3)$ in the

parameter regime studied by Rinzel and Keller [31]. Unfortunately this rules out direct quantitative comparison with their results. For instance, for $a > 0.15$ the parameter g should take values greater than 0.4 where $b = 1$, $\epsilon = 0.01$ and $D = 1$ (see Figure 4). Wave speed c is also monotonically increasing as we vary D (see Figure 6). It will aid our analysis later to consider the case $g = b$, and with $a = 0.1$, we see that travelling waves are supported and the velocity is monotonically increasing as the value of g (and b) increases (see Figure 7). This approach, whilst informative, is limited to finite, and low, generation levels of the $SG(3)$ lattice. It does however motivate us to develop an input-output renormalisation methodology which could inform us of the dispersive nature of the pre-fractal $SG(3)$ lattice at higher generation levels and ultimately on reaction-diffusion wave propagation on the $SG(3)$ fractal.

3. Green's Function Renormalisation for Fractal Lattices

The renormalisation approach affords the analysis of transport phenomena in heterogeneous structures via closed form solutions in terms of recursion relationships. One approach, which describes wave propagation on regular fractal lattices, uses aspects of graph theory to derive a discrete recursion relationship [29]. Such fractal models can be regarded as a family of graphs, which are defined by a recursive process,

$$\Psi^{(n+1)} = \Im[\Psi^{(n)}]. \tag{7}$$

Each graph consists of p copies of itself at level n to form its equivalent at level $n+1$. The adjacency matrix $H^{(n)}$, described in Section 2, captures the connectivity properties of the graph with its $(i,j)^{th}$ element giving the number of edges connecting site i to site j. The SG(3) graph considered in this paper has number of sites N_n and a constant number of edges emanating from each node. The recursive nature of this graph can be expressed as

$$H^{(n+1)} = \overline{H}^{(n)} + V^{(n)} \tag{8}$$

where $\overline{H}^{(n)}$ is a block diagonal matrix, whose blocks are equal to $H^{(n)}$, and $V^{(n)}$ is the connection matrix. $V^{(n)}$ is a sparse matrix, containing a constant number of nonzero elements. It represents the output nodes of $\Psi^{(n)}$ connected with each other during the recursive process to form $\Psi^{(n+1)}$. Thus we restrict our attention to study the case of a finitely ramified fractal. The Sierpinski Gasket lattice $SG(3)$ (see Figure 1) is the lattice counterpart of the Sierpinski gasket SG. The procedure starts from the SG of order 2 which consists of three filled triangle (see Figure 8). By taking one node at the centre of each of these triangles and then joining them together to get an equilateral triangle, we obtain the $SG(3)$ lattice at generation level $n = 1$. We can show that $SG(3)$ and SG have identical box counting and Hausdorff fractal dimension (see Appendix 1). As $n \to \infty$ the distance between nodes tends to zero and in this limit the lattice will perfectly match the space filling properties of the original Sierpinski Gasket.

3.1 Real Space Renormalisation Approach to the RK Model on the SG(3).

We start by detailing the matrix operators which are used to express the discretised RK model on $SG(3)$. We are interested in travelling wave solutions in the form of a step-like wave with $v = v^-$ for $z \to -\infty$, $v = v^+$ for $z \to +\infty$, $v^- < v^+$ with $z = x + ct$, where

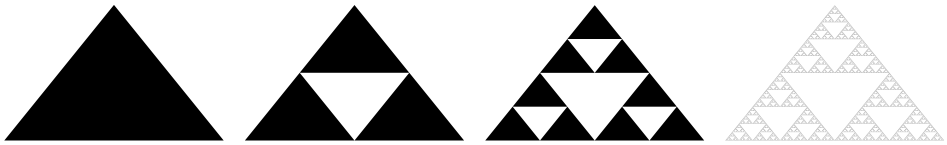

Figure 8: The first, second, third and seventh generation levels of the Sierpinski Gasket.

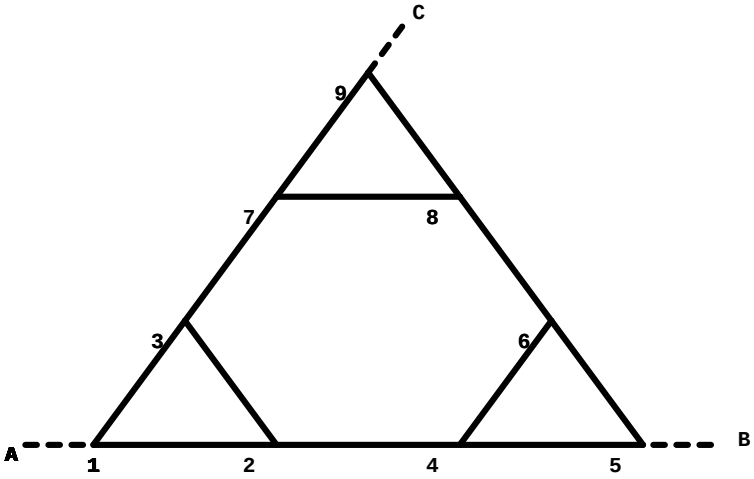

Figure 9: The Sierpinski Gasket lattice $SG(3)$ at level $n = 2$ of the $SG(3)$.Nodes 1, 5 and 9 are the input/output nodes. A, B and C are the fictitious nodes used to accommodate the boundary conditions.

c is the velocity of the wave front. System (3) can be written in terms of the variable z as follows,

$$\begin{aligned} c\frac{dv_i^{(n)}}{dz} &= D\nabla^2 v_i^{(n)} - g(f(v_i^{(n)}) + w_i^{(n)}) \\ c\frac{dw_i^{(n)}}{dz} &= bv_i^{(n)} \quad . \end{aligned} \tag{9}$$

Previous work which uses this renormalisation approach has transformed the field equations into the Laplace domain to cope with the time derivative [21]. Here however we are interested in analysing the dispersive properties of the $SG(3)$ and hence retain knowledge of the wave speed c. These two equations can be combined in one equation by taking the derivative with respect to z to give,

$$c\frac{d^2 v_i^{(n)}}{dz^2} = D\frac{d\nabla^2 v_i^{(n)}}{dz} - g\frac{df(v_i^{(n)})}{dz} - \frac{gb}{c}v_i^{(n)} \quad , \tag{10}$$

where the derivative is approximated by the local gradient to give,

$$\frac{df(v_i)}{dz} = \begin{cases} \dfrac{v_i - v_j + 1}{\triangle z} & \text{if } v_j > a \text{ and } v_i < a \\ \dfrac{v_i - v_j - 1}{\triangle z} & \text{if } v_i > a \text{ and } v_j < a \\ \dfrac{v_i - v_j}{\triangle z} & \text{Otherwise} \end{cases} . \tag{11}$$

Each of the operators in (3) is written in matrix form by discretising the independent variable z to give (see Appendix 2).

$$(\frac{c}{\triangle z^2}\sum_{i=1}^{N_n} R_{ij}^{(n)} - \frac{D}{\triangle z^3}\sum_{i=1}^{N_n} M_{ij}^{(n)} + \frac{g}{\triangle z}\sum_{i=1}^{N_n} K_{ij}^{(n)} + \frac{gb}{c}\sum_{i=1}^{N_n} I_{ij}^{(n)})v_j =$$
$$(\frac{-c}{\triangle z^2} - \frac{D}{\triangle z^3} + \frac{g}{\triangle z})v_A\delta_{1j} + (\frac{-c}{\triangle z^2} + \frac{D}{\triangle z^3})(v_B\delta_{mj} + v_C\delta_{N_nj})$$

for $j \in \{1, 2, \ldots, N_n\}$ where $I_{ij}^{(n)}$is the identity matrix. Alternatively in matrix form we have,

$$(\frac{c}{\triangle z^2}R^{(n)} - \frac{D}{\triangle z^3}M^{(n)} - + \frac{g}{\triangle z}K^{(n)} + \frac{gb}{c}I^{(n)})\underline{v} = (\frac{-c}{\triangle z^2} - \frac{D}{\triangle z^3} + \frac{g}{\triangle z})v_A\underline{e}_1$$
$$+ (\frac{-c}{\triangle z^2} + \frac{D}{\triangle z^3})(v_B\underline{e}_m + v_C\underline{e}_{N_n}). \tag{12}$$

Introduce the dimensionless ratio $\xi = \dfrac{\triangle z}{L}$ where $\triangle z$ represents the distance between any two neighbouring nodes and L is the characteristic size of the diffusing particles [25]. Non-dimensionalising equation (12), we obtain,

$$(\frac{Pe^2}{\phi^2}R^{(n)} - \frac{Pe}{\xi\phi^2}M^{(n)} + \xi PeK^{(n)} + \xi^2\phi^2 I^{(n)})\underline{v} = (\frac{-Pe^2}{\phi^2} - \frac{Pe}{\xi\phi^2} + \xi Pe)v_A\underline{e}_1$$
$$+(\frac{-Pe^2}{\phi^2} + \frac{Pe}{\xi\phi^2})(v_B\underline{e}_m + v_C\underline{e}_{N_n}). \tag{13}$$

where $Pe = \dfrac{cL}{D}$ is the Peclet number, $\phi = L\sqrt{\dfrac{g}{D}}$ is the Thiele modulus and for simplicity we set $g = b$. That is,

$$G^{(n)}\underline{v} = k_1 v_A\underline{e}_1 + k_2(v_B\underline{e}_m + v_C\underline{e}_{N_n}), \tag{14}$$

where
$G^{(n)} = \dfrac{Pe^2}{\phi^2}R^{(n)} - \dfrac{Pe}{\xi\phi^2}M^{(n)} + \xi PeK^{(n)} + \xi^2\phi^2 I^{(n)}$, $k_1 = \dfrac{-Pe^2}{\phi^2} - \dfrac{Pe}{\xi\phi^2} + \xi Pe$, and $k_2 = \dfrac{-Pe^2}{\phi^2} + \dfrac{Pe}{\xi\phi^2}$. To solve this set of linear equations in $\underline{v}$ we will calculate the Green's transfer matrix $F^{(n)} = (G^{(n)})^{-1}$ to give,

$$\underline{v} = F^{(n)}(k_1 v_A\underline{e}_1 + k_2(v_B\underline{e}_m + v_C\underline{e}_{N_n})). \tag{15}$$

Inverting G directly is computationally prohibitive and in addition we are interested in analysing the case $n \to \infty$. We can however develop a renormalisation approach which will provide the key elements of F at each generation level. The matrix $G^{(n+1)} = \overline{G}^{(n)} + T^{(n)}$, where $T^{(n)} = \dfrac{Pe^2}{\phi^2}R^{*(n)} - \dfrac{Pe}{\xi\phi^2}M^{*(n)} + \xi PeK^{*(n)}$, $n \geq 2$ is a sparse matrix defined as,

$$T_{ij}^{(n)} = \begin{cases} -k_1 = -\xi Pe + \frac{Pe}{\xi\phi^2} + \frac{Pe^2}{\phi^2} & \text{if } \{i,j\} \in S_1^n = \{\{1+3^n, \frac{3^n+1}{2}\}, \\ & \quad \{1+2\times 3^n, 3^n\}\} \\ -k_2 = \frac{-Pe}{\xi\phi^2} + \frac{Pe^2}{\phi^2} & \text{if } \{i,j\} \in S_2^n = \{\{\frac{3^n+1}{2}, 1+3^n\}, \{3^n, 1+2\times 3^n\}\}, \\ & \quad \{2\times 3^n, \frac{1+5\times 3^n}{2}\}, \{\frac{1+5\times 3^n}{2}, 2\times 3^n\}\} \\ 0 & \text{Otherwise} \end{cases}$$

and $\overline{G}^{(n)}$ is a block diagonal matrix of dimension $N_{n+1} \times N_{n+1}$, whose blocks equal $G^{(n)}$. The set of all nodes that have non-zero value of $T_{ij}^{(n)}$ is denoted by $S^{(n)} = S_1^{(n)} \bigcup S_2^{(n)}$. The following result gives the key renormalisation relationship:

Result 1

$$F^{(n+1)} = \overline{G}^{(n)} - \overline{G}^{(n)} T^{(n)} F^{(n+1)} \tag{16}$$

Proof (see Appendix 3)

The elements of $T^{(n)}$ represent the edges which connect the three copies of $F^{(n)}$ to generate $F^{(n+1)}$. Therefore it is a very sparse matrix and coupling this with the $SG(3)$ symmetry ensures a substantial reduction in the number of equations to be solved (see Appendix 4). We obtain a system of 14 coupled recursion relationships for the key elements of the Green function matrix which are sufficient to solve system (15). In the next section we will utilise this renormalisation scheme to investigate the case of finite generation level n.

4. Renormalisation Scheme for Finite Generation Levels of the $SG(3)$ Lattice.

In the last section we detailed an input-output renormalisation form for a Rinzel-Keller type reaction-diffusion system. At the heart of this methodology are the 14 recursion relationships which solve the system (15) for any generation level n. In this section we will look for travelling wave solutions by varying the parameters in system (15) for a range of finite generation levels, that is pre-fractal Sierpinski Gasket lattices.

4.1 The Boundary and Interface Conditions.

Our investigation will focus on finding a travelling wavefront solution moving with speed c. In equation (10), we have freedom to choose the origin $z = 0$ with $v(0) = a$ such that we have a region I where $v_i^I(z) < a$ and a region II where $v_i^{II}(z) > a$. Note that symmetry gives $v_B^I = v_C^I$ and $v_B^{II} = v_C^{II}$. We apply Neumann boundary conditions to the external input/output nodes in each region via,

$$v_A^I = v_1^I, \tag{17}$$

and

$$v_B^{II} = v_m^{II} \ . \tag{18}$$

We demand that the solution is smooth and continuous at the interface between regions I and II. The continuity condition between the two regions at the interface nodes gives,

$$v_B^I = v_1^{II} \tag{19}$$

and

$$v_A^{II} = v_m^I. \tag{20}$$

The smoothness condition, $\dfrac{dv_m^I}{dz} = \dfrac{v_1^{II}}{dz}$ implies $v_m^I - v_{m-1}^I = v_1^{II} - 1 - v_A^{II}$ and by (20) we get,

$$v_1^{II} - 2v_m^I + v_{m-1}^I = 0. \tag{21}$$

Note that equation (14) is defined in the two regions as,

$$G^{(n)}\underline{v}^I = k_1 v_A^I \underline{e}_1 + k_2(v_B^I \underline{e}_m + v_C^I \underline{e}_{N_n})$$

and

$$G^{(n)}\underline{v}^{II} = k_1(\frac{\xi Pe}{k_1} + v_A^{II})\underline{e}_1 + k_2(v_B^{II}\underline{e}_m + v_C^{II}\underline{e}_{N_n}).$$

The additional term in the equation for region II arises from the discontinuity in the operator K as defined in (11). Hence, equation (15) can be written, for any generation level n as,

$$v_i^{(n)I} = k_1 v_A^{(n)I} F_{i,1}^{(n)} + k_2 v_B^{(n)I} F_{i,m}^{(n)} + k_2 v_C^{(n)I} F_{i,N_n}^{(n)} \tag{22}$$

and

$$v_i^{(n)II} = k_1(\frac{\xi Pe}{k_1} + v_A^{(n)II})F_{i,1}^{(n)} + k_2 v_B^{(n)II} F_{i,m}^{(n)} + k_2 v_C^{(n)II} F_{i,N_n}^{(n)}, \tag{23}$$

for $i = 1, 2, \ldots N_n$. For clarity we will drop the generation level superscript (n). Taking into account the symmetry properties of the $SG(3)$ leads to a linear system of four equations with four unknowns v_A^I, v_B^I, v_A^{II}, v_B^{II} from equations (17) - (20),

$$v_A^{II} = \frac{(1 - k_2(F_{m,m} + F_{m,N_n}))}{k_1 F_{m,1}} v_B^{II} - \frac{\xi Pe}{k_1}, \tag{24}$$

$$v_A^I = \frac{2k_2 F_{1,m}}{1 - k_1 F_{1,1}} v_B^I, \tag{25}$$

$$v_B^I = F_{1,1}(1 - k_2(F_{m,m} + F_{m,N_n}))\frac{v_B^{II}}{F_{m,1}} + 2k_2 F_{1,m} v_B^{II}, \tag{26}$$

and

$$v_B^{II} = \frac{\xi Pe}{k_1}[\frac{1 - k_2(F_{m,m} + F_{m,N_n})}{k_1 F_{m,1}} - (\frac{2k_1 k_2 F_{m,1} F_{1,m}}{1 - k_1 F_{1,1}} + k_2(F_{m,m} + F_{m,N_n}))\times$$

$$(\frac{F_{1,1}(1 - k_2(F_{m,m} + F_{m,N_n}))}{F_{m,1}} + 2k_2 F_{1,m})]^{-1}. \tag{27}$$

The various terms in equation (21) have now been calculated apart from v_{m-1}^I. The node $m-1$ is the closest internal node to node m (see Figure 10). We need to calculate two pivotal values, denoted by $\hat{v}_A^{(2)I}$ and $\hat{v}_C^{(2)I}$, starting from the generation level n where

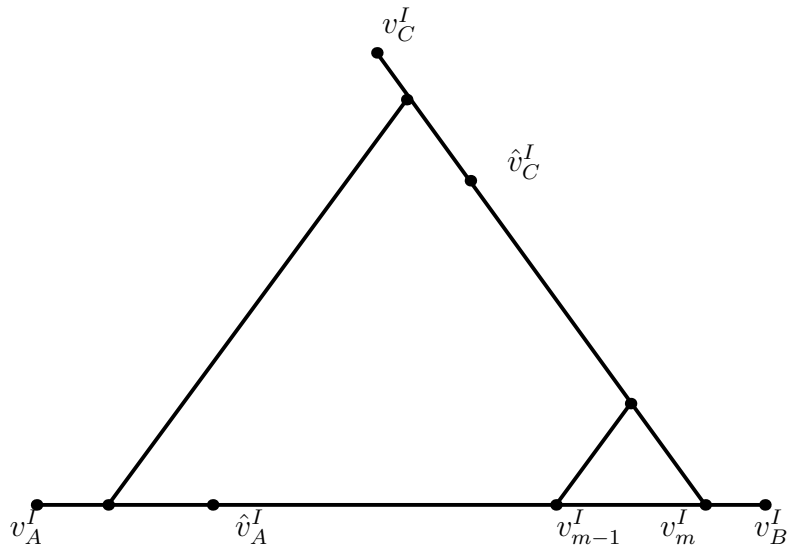

Figure 10: The value of the state variable v at the input/output nodes v_A^I, v_B^I and v_C^I and the pivotal values of v at nodes $\hat{v_A^I}$, $\hat{v_C^I}$, v_{m-1}^I and v_m^I in region I in the $SG(3)$ lattice structure.

$\hat{v}_A^{(n)I} = v_A^{(n)I}$ and $\hat{v}_C^{(n)I} = v_B^{(n)I}$. To calculate $\hat{v}_A^{(n-1)I}$ and $\hat{v}_C^{(n-1)I}$, for stage $p = n-1$ we have $m = 3^p + 1/2$ and $N_n = 3^p$ and so,

$$\hat{v}_A^{(p)I} = k_1 \hat{v}_A^{(p+1)I} F^{(p+1)}_{\frac{3^p+1}{2},1} + k_2 v_B^{(p+1)I} F^{(p+1)}_{\frac{3^p+1}{2},m} + k_2 \hat{v}_C^{(p+1)I} F^{(p+1)}_{\frac{3^p+1}{2},N_n} \tag{28}$$

$$\hat{v}_C^{(p)I} = k_1 \hat{v}_A^{(p+1)I} F^{(p+1)}_{2\times 3^p,1} + k_2 v_B^{(p+1)I} F^{(p+1)}_{2\times 3^p,N_n} + k_2 \hat{v}_C^{(p+1)I} F^{(p+1)}_{2\times 3^p,m} \ . \tag{29}$$

Note that $\hat{v}_C^{(n-1)I}$ should be the value at node $(5 \times 3^p + 1)/2$ and so we really want to calculate $k_1 \hat{v}_A^{(p+1)I} F^{(p+1)}_{\frac{5\times 3^p+1}{2},1} + k_2 v_B^{(p+1)I} F^{(p+1)}_{\frac{5\times 3^p+1}{2},m} + k_2 \hat{v}_C^{(p+1)I} F^{(p+1)}_{\frac{5\times 3^p+1}{2},N_n}$, but we have from symmetry that at any generation level p, $F_{\frac{5\times 3^p+1}{2},1} = F_{2\times 3^p+1,1}$, $F_{\frac{5\times 3^p+1}{2},m} = F_{\frac{2\times 3^p+1}{2},N_n}$ and $F_{\frac{5\times 3^p+1}{2},N_n} = F_{\frac{2\times 3^p+1}{2},m}$. Equation (28) and (29) are solved recursively until $p = 3$, that is generation level 2. Finally, v_{m-1}^I can be calculated as,

$$v_{m-1}^I = k_1 \hat{v}_A^{(2)I} F_{4,1} + k_2 \hat{v}_B^{(2)I} F_{4,5} + k_2 \hat{v}_C^{(2)I} F_{4,9}. \tag{30}$$

Then (21) can be written as,

$$k_1 F_{1,1}(1 + v_A^{II}) + 2k_2 F_{1,m} v_B^{II} - 2(k_1 F_{m,1} v_A^I + k_2 (F_{m,m} + F_{m,N_n}) v_B^I) + v_{m-1} = 0. \tag{31}$$

4.2 Results for Finite Generation Level.

All of the terms in equation (31) are ultimately functions of the dimensionless constants Pe, ϕ and the generation level n. By plotting equation (31) versus Pe and setting ϕ and the generation level n to certain values, we can identify our desired solutions (see Figure 11).

As can be seen there are many solutions but not all of these satisfy $v_i^I < a$ for all nodes i in region I and $v_i^{II} > a$ for all nodes i in region II, even though the interface and boundary conditions hold. This suggests that some additional monotonicity constraint

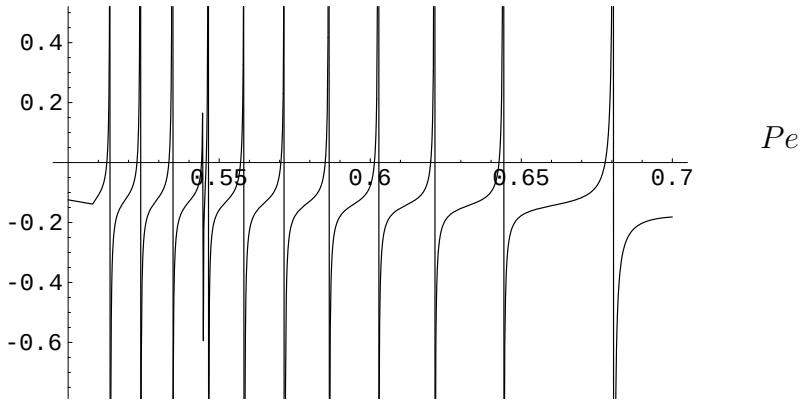

Figure 11: The smoothness equation (31) versus the Peclet number Pe where the Thiele modulus $\phi = 2.0$ and the generation level is $n = 8$.

needs to be imposed. This has inherent difficulties in implementation as, ostensibly we only have knowledge of the levels of each state variable at the input/output nodes and not at the internal nodes. However the calculation of v^I_{m-1} does provide some picture of monotonicity or otherwise of the solution. Therefore we can examine each of the solutions to (31) for this limited monotonicity property and then investigate the change in this particular solution as generation level increases. As the generation level increases, the solution changes less and less and appears to converge as n gets large (see Figure 12).

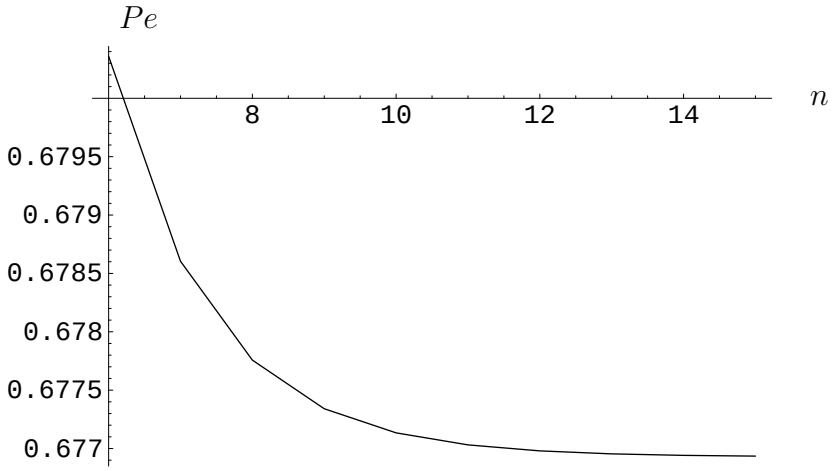

Figure 12: The Peclet number for a travelling wave-front solution versus the generation level $n = 6, 7, \cdots, 15$ where $\phi = 2$.

Of course the travelling wave solutions are driven by the renormalisation recursions. The convergence of this set of equations can be monitored by examining the change in the size of the vector $F^{(n)}_{i,j}$ from one generation level to the next. The L_2 norm difference $|\,\|F^{(n)}_{ij}\|_2 - \|F^{(n-1)}_{ij}\|_2|$ versus generation level n, shown in Figure 13, clearly converges to zero.

Importantly we can examine the relationship between the Peclet number (Pe) and the Thiele modulus (ϕ) for these travelling wave solutions. It can be seen in Figure 14

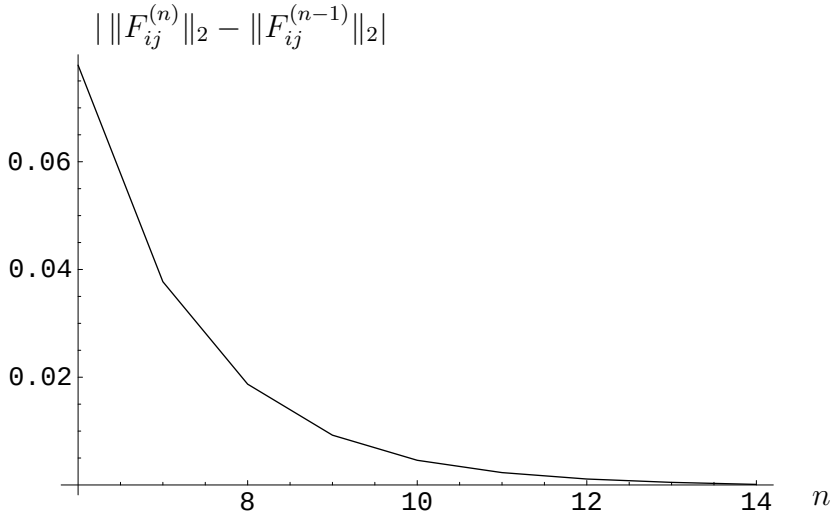

Figure 13: The behaviour of $|\,\|F_{ij}^{(n)}\|_2 - \|F_{ij}^{(n-1)}\|_2|$ as the generation level n increases for a travelling wave solution.

that the value of Pe is monotonically increasing as the value of ϕ increases for a fixed generation level n. It transpires that there are tight bounds on Pe due to the singularities that occur in equation (31), particularly as the generation level n increases. The results show that the $SG(3)$ can support travelling waves for finite generation levels which is in agreement with our finite difference approach in Section 2. More importantly is the quantitative comparison which can be achieved by examining the interdependency of the two dimensionless parameters Pe and ϕ.

Of course we can only make comparisons at low generation levels due to the prohibitive computational costs associated with the finite difference approach. Figure 14 compares a solution of the finite difference scheme with that obtained by the renomalisation approach. It can be seen that in both cases Pe increases as ϕ increases, and the values are of the same order of magnitude. There is a marked difference in the gradient of the essentially linear trend and the renormalisation method has a restricted range of values for ϕ. These differences are to be anticipated given the various assumptions associated with the renormalisation approach but are, at the same time, of such a level as to convince one of the utility of the renormalisation frame work. Particularly if one bears in mind that we can now examine relationships, such as that shown in Figure 14, for any generation level and ultimately, as $n \to \infty$, for the fractal $SG(3)$ lattice. There appears to be two classes of solutions which are driven by the behaviour of the renormalisation recursion equations. The recursion equations either converge to a fixed value or to a stable subspace of dimension 2, on whose domain the orbits appear to be chaotic. We will investigate this phenomenon elsewhere [34]. The results here suggest that the travelling wave associated with a specific (Pe, ϕ) regime will converge, as the generation level increases, to an invariant wave speed c. Therefore, as these pre-fractal supports tend to the actual fractal lattice $SG(3)$, the input-output renormalisation approach will afford an analysis of travelling waves, and this again will be discussed elsewhere [35].

5 Conclusions.

We have described in this paper an input/output renormalisation approach to the

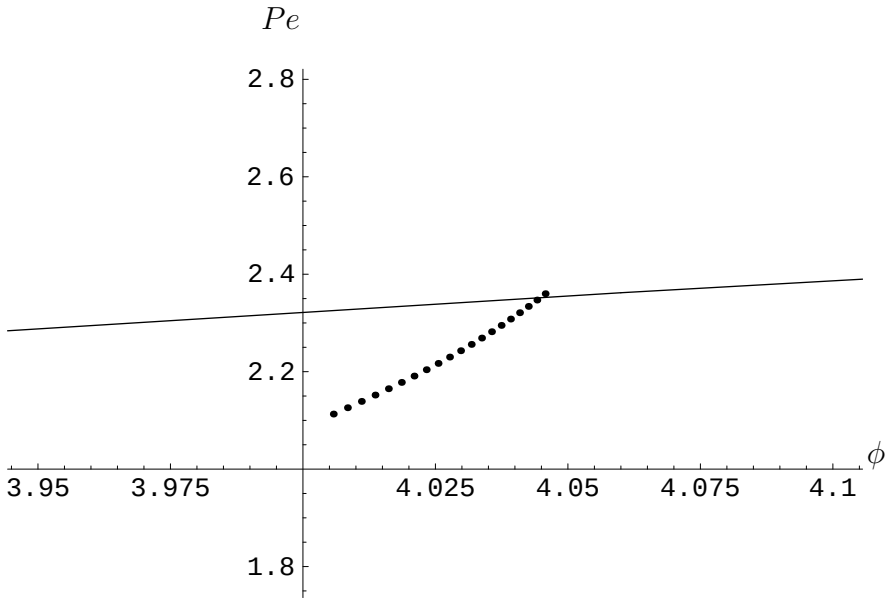

Figure 14: Pe versus ϕ for a travelling wave solution in the $SG(3)$ of order $n = 7$. The dashed line shows the relation found by the renormalisation approach whilst the continuous line is that obtained by the difference scheme (6). The initial value of ϕ was 2.36 and, for the finite difference approach, $a = 0.1$, $\epsilon = 0.01$, $D = 1$, $b = g$, $0.2 \leq g \leq 1.4$, $v_1^{(7)} = 1$ and total number of time steps $= 10^4$.

.

analysis of a coupled reaction-diffusion system in fractal media. In particular we have used a Rinzel-Keller (RK) type system to generate travelling waves on a Sierpinski gasket lattice ($SG(3)$). In order to motivate, inform and ultimately test this undertaking we first solved the system using a finite difference numerical scheme, for low generation levels of the fractal. We demonstrated that travelling waves were supported with the predominant structure being a planar wave. The piecewise linear nature of the reaction terms in the RK model render it amenable to a renormalisation approach. We have detailed the manner in which each operator is expressed discretely on the $SG(3)$. After nondimensionalisation, two key parameters emerge, the Peclet number (Pe) and the Thiele modulus (ϕ). Due to the symmetry and self-similarity properties of the fractal support the renormalisation scheme realises a set of fourteen recursion relationships, whose solution underlies the nature of each travelling wave. In this paper we have focused on deriving results for finite generation, or pre-fractal structures. Therefore we are able to compare our results with those obtained numerically using finite differences. Due to prohibitive computational costs the finite difference approach can only be carried out for low generation levels. The dimensionless parameters allow both qualitative and quantitative comparisons to be made. Considering the various assumptions which are required to realise a renormalisation solution the results compare very favourably. In physical applications one is invariably restricted to a finite range of length scales. The ability of the renormalisation scheme to generate solutions at the pre-fractal stage is therefore extremely important at a practical level.

The recursion relationships lying at the heart of the method can tend to a stable limit

or oscillate in a chaotic manner. We will fully describe the chaotic behaviour and its associated fractal repellor elsewhere [34]. The parameter regimes which achieve a stable limit are of particular theoretical importance, as in this limit, we are able to analyse reaction-diffusion wave propagation in a true fractal support. The existence and stability of such waves will be discussed in a future investigation [35].

References

[1] T. Vicsek, *Fractal Growth Phenomena*, 2nd ed. (World Scientific Pub. Co., Hong Kong, 1992).

[2] S. Havlin, M. Aroulo, H. LArralde, A. Shehter, H.F. Stanley and P. Trunfio, *Nuovo Cimento*, **16D(8)**, 1039 (1994).

[3] P.M. Adler, in *The Fractal Approach to Heterogeneous Chemistry*, 3rd ed., ed. D. Avnir, (John Wiley & Sons Ltd, New York, 1992), pp. 341-359.

[4] J.W. Haus and K.W. Kehr, *Physics Reports*, **150(5-6)**, 263 (1987).

[5] G. Zumofen, J. Klafter and A. Blumen, *Phys. Rev. A*, **44(12)**, 8390; *ibid* 8394 (1991).

[6] G. Zumofen, J. Klafter and A. Blumen, *J. Stat. Phys.*, **65(5/6)**, 1015 (1991).

[7] S.B. Yuste and K.Lindenberg, *Phys. Rev. Letts.*, **87(11)**, 118301 (2001).

[8] R. Metzler, W.G. Glockle and T.F. Nonnenmacher, *Physica A*, **211**, 13 (1994).

[9] B. O'Shaughnessy and I. Procaccia, *Phys. Rev. Letts.*, **54(5)**, 455 (1985).

[10] J. Kigami, *Trans. AMS*, **335(2)**, 721 (1993).

[11] M.L. Lapidus, in *Fractals in the Natural and Applied Sciences (A-41)*, ed., M.M. Novak, (Elsevier Science B.V., North-Holland, 1994), pp. 255-260.

[12] M. Yamaguti, M. Hata and J. Kigami, *Mathematics of Fractals*, (AMS Trans. of Math. Monographs, Rhode Island, Vol. 167, 1997).

[13] K.J. Falconer and J. Hu, *J. Math. Anal. Appl.*, **256**, 606 (2001).

[14] W.A. Schwalm and M.K. Schwalm, *Phys. Rev. B*, **37(16)**, 9525 (1988).

[15] W.A. Schwalm and M.K. Schwalm, *Phys. Rev. B*,**39(17)**, 12872 (1989).

[16] W.A. Schwalm and M.K. Schwalm, *Physica A*, **185**, 195 (1992).

[17] W.A. Schwalm and M.K. Schwalm, *Phys. Rev. B*, **47(13)**, 7847 (1993).

[18] Stauffer D. and Aharony A., *Introduction to Percolation Theory,* 2nd ed. (Taylor and Francis, London, 1994).

[19] A.R. Giona, M. Giona and L. Marrelli, *Chem. Eng. Sci.*, **47(9-11)**, 2623 (1992).

[20] M. Giona, *Chem. Eng. Sci.*, **47(6)**, 1503 (1992).

[21] M. Giona, *Chaos, Solitons and Fractals*, **7(9)**, 1371 (1996).

[22] M. Giona, *Fractals*, **5(3)**, 333 (1997).

[23] M. Giona, W.A. Schwalm, A. Adrover and M.K. Schwalm, *Chem. Eng. J.*, **64**, 45 (1996).

[24] M. Giona, W.A. Schwalm, M.K. Schwalm and A. Adrover, *Chem. Eng. Sci.*, **51(20)**, 4717 (1996).

[25] M. Giona, W.A. Schwalm, M.K. Schwalm and A. Adrover, *Chem. Eng. Sci.*, **51(20)**, 4731 (1996).

[26] M. Giona, A. Adrover, W.A. Schwalm and M.K. Schwalm, *Chem. Eng. Sci.*, **51(22)**, 5065 (1996).

[27] M. Giona, A. Adrover, W.A. Schwalm and M.K. Schwalm, *Fractals*, **5(3)**, 473 (1997).

[28] M. Giona and A. Adrover, *AIChE J*, **42(5)**, 1407 (1996).

[29] W.A. Schwalm, C.C. Reese, M.K. Schwalm and C.J. Wagner, *Phys. Letts. A*, **193**, 238 (1994).

[30] M.K. Schwalm, M. Giona, W.A. Schwalm, A. Adrover and M. Giustiniani, *Langmuir*, **13**, 1128 (1997).

[31] J. Rinzel and J.B. Keller, *Biophysical J.*, **13**, 1313 (1973).

[32] H.P. McKean, *Advances in Mathematics*, **4**, 209 (1970).

[33] P. Grindrod P., *Patterns and Waves*, 2nd ed. (Clarendon Press, Oxford, 1996).

[34] J. Abdulbake, A.J. Mulholland and J. Gomatam, (*in preparation*).

[35] J. Abdulbake, A.J. Mulholland and J. Gomatam, (*in preparation*).

[36] K. Falconer, *Fractal Geometry*,(John Wiley and Sons, Chichester, UK, 1990).

Appendix 1. The Sierpinski gasket lattice SG(3)

Let the set F denote the Sierpinski gasket lattice with Hausdorff dimension $dim_H F$ and the box counting dimension $dim_B F$, then

$$\dim_H F = \dim_B F = \frac{\log 3}{\log 2}.$$

Proof.

In general, the pre-fractal set E_k has $N_{\delta_k} = \frac{3}{2}(3^k - 1)$ edges of length $\delta_k = \dfrac{1}{2^{k+1} - 1}$ and 3^{k+1} nodes. Using definition (iv), p41 of [36], let $N_{\delta_k}(F)$ be the smallest number of sets with diameter at most δ_k that cover F. As $k \to \infty$, $\delta_k \to 0$ and we have,

$$\begin{aligned}
\overline{\dim}_B F = \lim_{\delta_k \to 0} \sup \frac{\log N_{\delta_k}(F)}{-\log \delta_k} &\leq \lim_{k \to \infty} \sup \frac{\log \frac{3}{2}(3^k - 1)}{\log(2^{k+1} - 1)} \\
&\leq \lim_{k \to \infty} \sup \frac{\log \frac{3}{2} \times 3^{k+1}}{\log 2^k} \\
&= \lim_{k \to \infty} \sup \frac{\log \frac{3}{2}}{k \log 2} + (1 + \frac{1}{k}) \frac{\log 3}{\log 2} = \frac{\log 3}{\log 2}.
\end{aligned}$$

Now using definition (v), p41 of [36], let N_{δ_k} be the largest number of disjoint balls of radius δ_k, with centres in F. The number of disjoint balls of radius $\delta_k = \frac{1}{2}(\frac{1}{2^{k+1}-1})$ centred at each node of F is 3^{k+1}. Hence

$$\begin{aligned}
\underline{\dim}_B F = \lim_{\delta_{k \to 0}} \inf \frac{\log N_{\delta_k}(F)}{-\log \delta_k} &\geq \lim_{k \to \infty} \inf \frac{\log 3^{k+1}}{\log 2(2^{k+1} - 1)} \\
&\lim_{k \to \infty} \inf \frac{(k+1) \log 3}{(k+2) \log 2} \\
&= \lim_{k \to \infty} \inf \frac{(1 + \frac{1}{k}) \log 3}{(1 + \frac{2}{k}) \log 2} = \frac{\log 3}{\log 2}
\end{aligned}$$

which implies that,

$$\frac{\log 3}{\log 2} \leq \underline{dim}_B F \leq \dim_B F \leq \overline{dim}_B F \leq \frac{\log 3}{\log 2}.$$

Thus $\dim_B F = \dfrac{\log 3}{\log 2}$.

Let μ be the mass distribution on the F such that each of the $\dfrac{3}{2}(3^k - 1)$ edges of side length $\dfrac{1}{2^{k+1} - 1}$ in E_k carries a mass of $\dfrac{2}{3(3^k - 1)}$. If $2^{-(k+2)} \leq |U| < 2^{-(k+1)}$ for some $k \geq 1$, then U can intersect at most 3 of the edges in E_k, and so,

$$\mu(U) \leq \frac{3 \times 2}{3(3^k - 1)} \leq \frac{2}{3^{k-1}}$$

$$= 54 \times 2^{-(k+1)\frac{\log 3}{\log 2}} \leq 54|U|^{\log 3/\log 2}.$$

So by the mass distribution principle, p55 of [36], we get,

$$\frac{\log 3}{\log 2} \leq dim_H F \leq \underline{dim}_B F \leq \overline{dim}_B F.$$

We have already shown that $\dim_B F = \dfrac{\log 3}{\log 2}$ and so $\dim_H F = \dfrac{\log 3}{\log 2}$.

Appendix 2. Discretisation of the Operators

We formulate each of the matrices in equation (3) at generation level $n = 2$ (see Figure 9). We introduce three fictitious nodes, A, B and C corresponding to the input/output nodes which, in general for any order n, are coded by 1, m and N_n respectively, where $m = \frac{N_n+1}{2}$. For notational clarity we will only use the generation level superscript (n) on v where it is absolutely necessary. The value of v at each fictitious node is denoted by v_A, v_B and v_C. For instance, for level $n = 2$, the fictitious nodes A, B and C are connected to the input/output nodes 1, 5 and 9 respectively.

We express the operator $\dfrac{df(v_i)}{dz}$ as $\dfrac{K\underline{v}}{\triangle z}$ where, if we assume for clarity at this stage that all values of v_j are greater than a,

$$K^{(2)}v_i = \quad v_i - v_p \quad \text{where, } \{i,p\} \in \{\{1,A\},\{2,1\},\{3,1\},\{2,4\},\{5,4\} \\ ,\{6,4\},\{7,3\},\{8,7\},\{9,7\}\}$$

.

Note we define $K^{(2)}_{Bj}$ using $K^{(2)}_{Bj}v_j = v_B - v_m$ and similarly $K^{(2)}_{Cj}$ using $K^{(2)}_{Cj}v_j = v_C - v_{N_n}$. For any level $n \geq 3$,

$$K^{(n+1)}_{ij} = \overline{K}^{(n)}_{ij} + K^{*(n)}_{ij}$$

where $\overline{K}^{(n)}_{ij}$ is a block diagonal matrix defined by,

$$\overline{K}^{(n)}_{pq} = \begin{cases} K^{(2)}_{(p-1)mod9+1,(q-1)mod9+1} & \text{if} \lceil p/9 \rceil = \lceil q/9 \rceil \text{ for } p,q \in \{1,\cdots,N_n = 3^n\} \\ 0 & \text{Otherwise} \end{cases},$$

$K^{*(n)}_{ij}$ is a sparse matrix defined by,

$$K^{*(n)}_{ij} = \begin{cases} -1 & \{p,q\} \in Q^-_n \\ 0 & \text{Otherwise} \end{cases},$$

and $Q_n = Q^+_n \bigcup Q^-_n$ where,

$$Q^-_n = \begin{cases} \bigcup_{i=4}^{n} \{W^{-(i)}, Q^-_{i-1}, Q^-_{i-1} + 3^{i-1}, Q^-_{i-1} + 2 \times 3^{i-1}\} & \text{, for } n \geq 4 \\ W^{-(3)} & \text{if } n = 3 \end{cases},$$

$$Q_n^+ = \begin{cases} \bigcup_{i=4}^{n}\{W^{+^{(i)}}, Q_{i-1}^+, Q_{i-1}^+ + 3^{i-1}, Q_{i-1}^+ + 2\times 3^{i-1}\} & \text{, for } n \geq 4 \\ W^{+^{(3)}} & \text{if } n = 3 \end{cases}$$

and

$$Q_n = \begin{cases} \bigcup_{i=4}^{n}\{W^{(i)}, Q_{i-1}, Q_{i-1} + 3^{i-1}, Q_{i-1} + 2\times 3^{i-1}\} & \text{, for } n \geq 4 \\ W^{(3)} & \text{if } n = 3 \end{cases}.$$

Also $W_n = W_n^+ \bigcup W_n^-$ where,

$$\begin{aligned} W^{(n)} &= \{\{(3^{n-1}+1)/2, 1+3^{n-1}\}, \{3^{n-1}, 1+2\times 3^{n-1}\}, \{2\times 3^{n-1}, (5\times 3^{n-1}+1)/2\}, \\ &\quad \{1+3^{n-1}, (3^{n-1}+1)/2\}, \{1+2\times 3^{n-1}, 3^{n-1}\}, \{(5\times 3^{n-1}+1)/2, 2\times 3^{n-1}\}\}, \end{aligned}$$

$$\begin{aligned} W^{+^{(n)}} &= \{\{(3^{n-1}+1)/2, 1+3^{n-1}\}, \{3^{n-1}, 1+2\times 3^{n-1}\}, \\ &\quad \{2\times 3^{n-1}, (5\times 3^{n-1}+1)/2\}, \{(5\times 3^{n-1}+1)/2, 2\times 3^{n-1}\}\}, \end{aligned}$$

and

$$W^{-^{(n)}} = \{\{1+3^{n-1}, (3^{n-1}+1)/2\}, \{1+2\times 3^{n-1}, 3^{n-1}\}\}.$$

The operator $\frac{d^2 v_i^{(n)}}{dz^2}$ is expressed in discrete form as $\frac{R\underline{v}}{\triangle z^2}$. where, the i^{th} row of $R^{(2)}$ is defined in terms of $K^{(2)}$ as,

$$R_{ij}^{(2)} = \begin{cases} \frac{1}{2}(K_{3j}^{(2)} + K_{2j}^{(2)}) - K_{1j}^{(2)} & \text{if, } i = 1 \\ K_{pj}^{(2)} - K_{ij}^{(2)} & \text{if } \{i,p\} \in \{\{2,4\},\{3,7\},\{4,5\},\{5,B\},\{7,9\},\{9,C\}\} \\ K_{ij}^{(2)} - K_{pj}^{(2)} & \text{if, } \{i,p\} \in \{\{6,4\},\{8,7\}\} \end{cases},$$

for $j = 1, 2, \ldots, 9$. Defining $R_{ij}^{(2)}$ in this way, ensures that only the input/output nodes use the fictitious nodes, the symmetry in the wave front about the median from node 1 is maintained, and $R_{ij}^{(2)}$ is non-singular. In general, for any level $n \geq 3$,

$$R_{ij}^{(n+1)} = \overline{R}_{ij}^{(n)} + R_{ij}^{*(n)},$$

where $\overline{R}_{ij}^{(n)}$ is a block diagonal matrix define by,

$$\overline{R}_{pq}^{(n)} = \begin{cases} R_{(p-1)mod9+1,(q-1)mod9+1}^{(2)} & \text{if } \lceil p/9 \rceil = \lceil q/9 \rceil \text{ for } p,q \in \{1,\ldots,N_n = 3^n\} \\ 0 & \text{Otherwise} \end{cases}$$

and $R_{ij}^{*(n)}$ is a sparse matrix defined by,

$$R_{pq}^{*^{(n)}} = \begin{cases} 1 & \{p,q\} \in Q_n \\ 0 & \text{Otherwise} \end{cases}.$$

The operator $\frac{d\nabla^2 v_i^{(n)}}{dz^3}$ has discrete representation $\frac{M\underline{v}}{\triangle z^3}$, where the i^{th} row of M is defined using the Laplacian operator matrix (4) with $B_{pq}^{(n)} = 0$,for generation level $n = 2$ as

$$M_{ij}^{(2)} = \begin{cases} \frac{1}{2}(A_{2j}^{(2)} + A_{3j}^{(2)}) - A_{1j}^{(2)} & \text{if } i = 1 \\ A_{pj}^{(2)} - A_{ij}^{(2)} & \text{if } \{i,p\} \in \{\{2,4\},\{3,7\}\} \\ A_{ij}^{(2)} - A_{pj}^{(2)} & \text{if } \{i,p\} \in \{\{4,2\},\{5,4\},\{6,4\},\{7,3\},\{8,7\},\{9,7\}\} \end{cases},$$

for $j = 1, 2, \ldots, 9$. As before, we must define M at each node carefully to ensure that only one fictitious node is required for each input/output node, that wave front symmetry is maintained and that the internal nodes do not use any of the fictitious nodes. In general, for any level $n \geq 3$,

$$M_{ij}^{(n+1)} = \overline{M}_{ij}^{(n)} + M_{ij}^{*(n)},$$

where $\overline{M}_{ij}^{(n)}$ is a block diagonal matrix defined by,

$$\overline{M}_{pq}^{(n)} = \begin{cases} M_{(p-1)mod9+1,(q-1)mod9+1}^{(2)} & \text{if } \lceil p/9 \rceil = \lceil q/9 \rceil \text{ for } p,q \in \{1,\ldots,N_n = 3^n\} \\ 0 & \text{Otherwise} \end{cases}.$$

$M_{ij}^{*(n)}$ is a sparse matrix defined by,

$$M_{pq}^{*(n)} = \begin{cases} 1 & \{p,q\} \in Q_n^+ \\ -1 & \{p,q\} \in Q_n^- \\ 0 & \text{Otherwise} \end{cases}$$

Appendix 3. Proof of Result 1

Result 1

$$F^{(n+1)} = \overline{G}^{(n)} - \overline{G}^{(n)} T^{(n)} F^{(n+1)} \tag{32}$$

Proof

$F^{(n)^{-1}} = \frac{Pe^2}{\phi^2} R^{(n)} - \frac{Pe}{\xi\phi^2} M^{(n)} + \xi Pe K^{(n)} + \xi^2\phi^2 I^{(n)}.$
Since $\overline{G}^{(n)}$ is a block diagonal matrix $\overline{G}^{(n)^{-1}} = \overline{G^{(n)^{-1}}}$, which gives,
$\overline{G}^{(n)^{-1}} = \frac{Pe^2}{\phi^2} \overline{R}^{(n)} - \frac{Pe}{\xi\phi^2} \overline{M}^{(n)} + \xi Pe \overline{K}^{(n)} + \xi^2\phi^2 I^{(n+1)}).$
Also we have, $R^{(n+1)} = \overline{R}^{(n)} + R^{*^{(n)}}$, $M^{(n+1)} = \overline{M}^{(n)} + M^{*^{(n)}}$ and $K^{(n+1)} = \overline{K}^{(n)} + K^{*^{(n)}}$ which imply that,
$F^{(n+1)^{-1}} = \frac{Pe^2}{\phi^2}(\overline{R}^{(n)} - R^{*^{(n)}}) - \frac{Pe}{\xi\phi^2}(\overline{M}^{(n)} - M^{*^{(n)}}) + \xi Pe(\overline{K}^{(n)} - K^{*^{(n)}}) + \xi^2\phi^2 I^{(n+1)}.$
Now,

$$
\begin{aligned}
I_{N_{n+1}\times N_{n+1}} = & \quad \overline{G}^{(n)}\overline{G}^{(n)^{-1}} \\
= & \quad \overline{G}^{(n)}(\frac{Pe^2}{\phi^2}\overline{R}^{(n)} - \frac{Pe}{\xi\phi^2}\overline{M}^{(n)} \\
& \quad +\xi Pe\overline{K}^{(n)} + \xi^2\phi^2 I^{(n+1)}) \\
= & \quad \overline{G}^{(n)}(\frac{Pe^2}{\phi^2}(R^{(n+1)} - R^{*^{(n)}}) - \frac{Pe}{\xi\phi^2}(M^{(n+1)} - M^{*^{(n)}}) \\
& \quad +\xi Pe(K^{(n+1)} - K^{*^{(n)}}) + \xi^2\phi^2 I^{(n+1)}) \\
= & \quad \overline{G}^{(n)}(\frac{Pe^2}{\phi^2}R^{(n+1)} - \frac{Pe}{\xi\phi^2}M^{(n+1)} + \xi PeK^{(n+1)} + \xi^2\phi^2 I^{(n+1)} \\
& \quad -(\frac{Pe^2}{\phi^2}R^{*^{(n)}} - \frac{Pe}{\xi\phi^2}M^{*^{(n)}} + \xi PeK^{*^{(n)}})) \\
= & \quad \overline{G}^{(n)}(F^{(n+1)^{-1}} - T^{(n)}) \\
= & \quad (\overline{G}^{(n)} - \overline{G}^{(n)}T^{(n)}F^{(n+1)})F^{(n+1)^{-1}}.
\end{aligned}
$$

Therefore, $F^{(n+1)} = \overline{G}^{(n)} - \overline{G}^{(n)}T^{(n)}F^{(n+1)}$.

Appendix 4. The Renormalisation Recursive Equations.

To utilise the recursive relationship (16) the $SG(3)$ at level $n = 2$, that is $N_n = 9$, is considered as an initial structure. The Green functions $F^{(2)}_{ij}$ are calculated by directly inverting $G^{(2)}_{ij}$. For simplicity, we detail the calculation of the pivotal elements at generation level 3. The Green function at level $n = 2$ is denoted by $f_{i,j}$ and for the next generation, it is denoted by $F^{(3)}_{i,j}$. Due to the symmetry, at level $n = 2$, we have $f_{1,5} = f_{1,9}$, $f_{5,1} = f_{9,1}$, $f_{5,5} = f_{9,9}$ and $f_{5,9} = f_{9,5}$. The corresponding Green functions carry this symmetry forward to each level n. This means that for level $n = 3$ we have, $F^{(3)}_{1,14} = F^{(3)}_{1,27}$, $F^{(3)}_{14,1} = F^{(3)}_{27,1}$, $F^{(3)}_{14,14} = F^{(3)}_{27,27}$ and $F^{(3)}_{14,27} = F^{(3)}_{27,14}$. There are other minor symmetries which will be considered when they arise below. Now,

$$
\begin{aligned}
F^{(3)}_{1,1} &= \overline{G}^{(2)}_{1,1} - \sum_{\{h,k\}\in S^{(2)}} \overline{G}^{(2)}_{1,h}T^{(2)}_{h,k}F^{(3)}_{k,1} \\
&= \overline{G}^{(2)}_{1,1} - (\overline{G}^{(2)}_{1,5}T^{(2)}_{5,10}F^{(3)}_{10,1} + \overline{G}^{(2)}_{1,9}T^{(2)}_{9,19}F^{(3)}_{19,1}) \\
&= f_{1,1} + k_2 f_{1,5}F^{(3)}_{10,1} + k_2 f_{1,9}F^{(3)}_{19,1} \ .
\end{aligned}
$$

Since $f_{1,9} = f_{1,5}$ and, due to symmetry, $F^{(3)}_{19,1} = F^{(3)}_{10,1}$, we find,

$$
F^{(3)}_{1,1} = f_{1,1} + 2k_2 f_{1,5}F^{(3)}_{10,1} \ . \tag{33}
$$

Now the element $F^{(3)}_{10,1}$ is calculated in a similar way to give,

$$
F^{(3)}_{10,1} = k_1 f_{1,1}F^{(3)}_{5,1} + k_2 f_{1,5}F^{(3)}_{18,1} \ . \tag{34}
$$

Continuing in this way the element $F^{(3)}_{18,1}$ can be calculated as,

$$F^{(3)}_{18,1} = k_1 f_{5,1} F^{(3)}_{5,1} + k_2 f_{5,5} F^{(3)}_{18,1} \ . \tag{35}$$

Also,

$$F^{(3)}_{5,1} = f_{5,1} + k_2 (f_{5,5} + f_{5,9}) F^{(3)}_{10,1} \ . \tag{36}$$

The equations (33), (34), (35) and (36) represent a system of four linear equations with four unknowns, $F^{(3)}_{1,1}$, $F^{(3)}_{10,1}$, $F^{(3)}_{18,1}$ and $F^{(3)}_{5,1}$. The element $F^{(3)}_{14,1}$ can now be calculated as,

$$F^{(3)}_{14,1} = k_1 f_{5,1} F^{(3)}_{5,1} + k_2 f_{5,9} F^{(3)}_{18,1}, \tag{37}$$

and $F^{(3)}_{1,14}$ as,

$$F^{(3)}_{1,14} = k_2 f_{1,5} F^{(3)}_{10,14} + k_2 f_{1,5} F^{(3)}_{10,27}. \tag{38}$$

Similarly,

$$F^{(3)}_{10,14} = f_{1,5} + k_1 f_{1,1} F^{(3)}_{5,14} + k_2 f_{1,5} F^{(3)}_{18,27} \ , \tag{39}$$

$$F^{(3)}_{10,27} = k_1 f_{1,1} F^{(3)}_{5,27} + k_2 f_{1,5} F^{(3)}_{18,14} \ , \tag{40}$$

$$F^{(3)}_{5,14} = k_2 f_{5,5} F^{(3)}_{10,14} + k_2 f_{5,9} F^{(3)}_{10,27} \ , \tag{41}$$

$$F^{(3)}_{18,27} = k_1 f_{5,1} F^{(3)}_{5,27} + k_2 f_{5,5} F^{(3)}_{18,14} \ , \tag{42}$$

$$F^{(3)}_{5,27} = k_2 f_{5,5} F^{(3)}_{10,27} + k_2 f_{5,9} F^{(3)}_{10,14} \ , \tag{43}$$

$$F^{(3)}_{18,14} = f_{5,9} + k_1 f_{5,1} F^{(3)}_{5,14} + k_2 f_{5,5} F^{(3)}_{18,27} \ , \tag{44}$$

$$F^{(3)}_{14,14} = f_{5,5} + k_1 f_{5,1} F^{(3)}_{5,14} + k_2 f_{5,9} F^{(3)}_{18,27} \ , \tag{45}$$

and

$$F^{(3)}_{14,27} = k_1 f_{5,1} F^{(3)}_{5,27} + k_2 f_{5,9} F^{(3)}_{18,14} \ . \tag{46}$$

The seven equations (38)-(44) represent a linear system with seven unknowns $F^{(3)}_{1,14}$, $F^{(3)}_{10,14}$, $F^{(3)}_{10,27}$, $F^{(3)}_{5,14}$, $F^{(3)}_{5,27}$, $F^{(3)}_{18,14}$ and $F^{(3)}_{18,27}$. Subsequently, $F^{(3)}_{14,14}$ and $F^{(3)}_{14,27}$ can be calculated from (45) and (46).